# Proof of concept for low-dose molecular breast imaging with a dual-head CZT gamma camera. Part I. Evaluation in phantoms

Carrie B. Hruska,[a] Amanda L. Weinmann, and Michael K. O'Connor
*Department of Radiology, Mayo Clinic, 200 First Street SW, Rochester, Minnesota 55905*

(Received 2 December 2011; revised 1 May 2012; accepted for publication 2 May 2012; published 29 May 2012)

**Purpose:** Molecular breast imaging (MBI) is a nuclear medicine technology that uses dual-head cadmium zinc telluride (CZT) gamma cameras to image functional uptake of a radiotracer, Tc-99m sestamibi, in the breast. An important factor in adoption of MBI in the screening setting is reduction of the necessary administered dose of Tc-99m sestamibi from the typically used dose of 740 MBq to approximately 148 MBq, such that MBI's whole-body effective dose is comparable to that of screening mammography. Methods that increase MBI count sensitivity may allow a proportional reduction in the necessary administered dose. Our objective was to evaluate the impact of two count sensitivity improvement methods on image quality by evaluating count sensitivity, spatial resolution, and lesion contrast in phantom simulations.

**Methods:** Two dual-head CZT-based MBI systems were studied: LumaGem and Discovery NM 750b. Two count sensitivity improvement methods were implemented: registered collimators optimized for dedicated breast imaging and widened energy acceptance window optimized for use with CZT. System sensitivity, spatial resolution, and tumor contrast-to-noise ratio (CNR) were measured comparing standard collimation and energy window setting [126–154 keV (+10%, −10%)] with optimal collimation and a wide energy window [110–154 keV (+10%, −21%)].

**Results:** Compared to the standard collimator designs and energy windows for these two systems, use of registered optimized collimation and wide energy window increased system sensitivity by a factor of 2.8–3.6. Spatial resolution decreased slightly for both systems with new collimation. At 3 cm from the collimator face, LumaGem's spatial resolution was 4.8 and 5.6 mm with standard and optimized collimation; Discovery NM 750b's spatial resolution was 4.4 and 4.6 mm with standard and optimized collimation, respectively. For both systems, at tumor depths of 1 and 3 cm, use of optimized collimation and wide energy window significantly improved CNR compared to standard settings for tumors 8.0 and 9.2 mm in diameter. At the closer depth of 1 cm, optimized collimation and wide energy window also significantly improved CNR for 5.9 mm tumors on Discovery NM 750b.

**Conclusions:** Registered optimized collimation and wide energy window yield a substantial gain in count sensitivity and measurable gain in CNR, with some loss in spatial resolution compared to the standard collimator designs and energy windows used on these two systems. At low-count densities calculated to represent doses of 148 MBq, this tradeoff results in adequate count density and lesion contrast for detection of lesions ≥8 mm in the middle of a typical breast (3 cm deep) and lesions ≥6 mm close to the collimator (1 cm deep).  [http://dx.doi.org/10.1118/1.4718665]

Key words: breast cancer, molecular breast imaging, gamma camera, radiation risk, count sensitivity

## I. INTRODUCTION

Molecular breast imaging (MBI) is a nuclear medicine procedure that employs a dedicated dual-head gamma camera for imaging uptake of a radiopharmaceutical, typically Tc-99m sestamibi, in the breast. Using pixilated semiconductor [cadmium zinc telluride (CZT)]-based detectors specifically optimized for breast imaging, MBI has demonstrated the ability to reliably detect breast tumors in a variety of diagnostic settings.[1,2] Detection of breast cancer with MBI relies on differences in functional uptake of Tc-99m sestamibi, rather than differences in the attenuation coefficients of tissues in the breast as with mammography. We are therefore studying MBI as a possible adjunct technique to screening mammography for women with radiographically dense breasts, a population in whom the sensitivity of mammography is reduced.[3–7]

Hendrick recently evaluated the radiation-induced cancer risks associated with two other nuclear medicine breast imaging techniques, breast specific gamma imaging (BSGI) and positron emission mammography (PEM).[8] BSGI and MBI both detect single photon emissions from the radiotracer Tc-99m sestamibi. BSGI and MBI techniques are similar in many respects but differ in both the detector technology and configuration. BSGI utilizes a single camera multicrystal sodium iodide detector, whereas MBI employs two cameras with CZT detectors. PEM comprises a pair of detectors

operating in coincidence to image positron emissions from 18F-fluorodeoxyglucose (FDG).

BSGI studies typically employ 925–1110 MBq Tc-99m sestamibi, resulting in a whole-body effective dose of 7.8–9.4 mSv. PEM studies typically use 370 MBq F-18 FDG, resulting in effective dose of ~6.7 mSv. The effective doses for a two-view bilateral mammogram are a factor of 10–20 times less, at 0.44 mSv for digital mammography and 0.56 mSv for film.[8] Using BEIR VII age-dependent risk data,[9] the lifetime attributable risk of inducing fatal cancer due to a single BSGI or PEM study performed with the administered doses given above was calculated as 20–30 times that of a mammogram in a woman aged 40 yr.

A similar analysis by O'Connor *et al.*[10] concluded that in order for radiotracer-based techniques to have radiation-induced cancer risks comparable to that of mammography, the injected radiotracer activities must be reduced to 148 MBq or less of Tc-99m sestamibi and 111 MBq or less of F-18 FDG. These injected doses correspond to an effective radiation dose of 1.2 mSv. With expected screening intervals of 2–3 yr for MBI, this radiation dose would be comparable to that received from annual screening mammography. The low radiation doses received from annual screening mammography programs have been determined to be of low risk compared with expected mortality reductions achievable through mammographic screening.[11]

In an effort to reduce the necessary administered dose for MBI from the 740 MBq typically administered at our institution to 148 MBq Tc-99m sestamibi or less, we have optimized the gamma camera collimator design and applied a wider energy acceptance window with the aim of increasing system sensitivity while retaining the high spatial resolution of this technique.[12–14] Gains in count sensitivity may allow a proportional reduction in the necessary administered dose. The goal of this work was to evaluate the impact of these two sensitivity improvement methods on image quality by evaluating count sensitivity, spatial resolution, and lesion contrast in phantom simulations.

## II. MATERIALS AND METHODS

### II.A. Molecular breast imaging systems

Two MBI gamma cameras are under study at our institution: the LumaGem [Gamma Medica-Ideas (GMI), Northridge, CA] and the Discovery NM 750b [General Electric (GE) Medical Systems, Haifa, Israel]. Both systems comprise dual-head pixilated CZT detectors mounted on a modified mammographic gantry. The LumaGem system has a 20 cm × 16 cm field of view, a pixel size of 1.6 mm and energy resolution of ~4%. The Discovery NM 750b has a 20 cm × 20 cm field of view, a 2.5 mm pixel size and an energy resolution of ~6.5%. Both systems have ~7–8 mm dead space at the edge of the field of view, permitting the breast to be positioned directly on the detector face in a position analogous to that of mammography. The dual-head design of these CZT detectors was previously shown to significantly increase detection of small breast lesions compared to a single CZT detector.[15]

### II.B. Methods for increased sensitivity

Two sensitivity improvement methods were implemented with the goal of increasing count sensitivity while maintaining adequate spatial resolution for detection of small tumors: collimator optimization and widened energy acceptance window.

#### *II.B.1. Collimator optimization*

We have previously reported on theoretical calculations and Monte Carlo simulations performed to optimize the collimator designs for the LumaGem and Discovery NM 750b detectors.[12] The new collimator designs were registered so that each hole was matched to an individual CZT pixel on each detector system. Collimator designs were constrained by the fixed pixel sizes of the detectors, and by the requirement of a system spatial resolution of ≤5 mm at a distance of 3 cm from the collimator face. This requirement was based on analysis of 128 tumors in 150 patient studies performed in our laboratory, which demonstrated that less than 12% of tumors detected were <5 mm in size, and 59% were in the 6–15 mm range.[15] Average compressed breast thickness in two previous studies was 5.5–6.0 cm.[15,16] Hence, with two opposing dual-head detectors, the collimators were designed to achieve a spatial resolution of ≤5 mm in the middle of a 6-cm compressed breast. Using these constraints, theoretical calculations and results from Monte Carlo simulations indicated that count sensitivity could be improved by a factor of 1.5 compared to the sensitivity of these detector systems with their original collimators.[12] This improvement did not include any additional benefits that might accrue from matching of the collimators to the pixels.

Based on these previous findings, new optimized collimators were constructed by Creatv Technologies (Potomac, MD) for the LumaGem, and Kolscint (Tefen, Israel) for the Discovery NM 750b. The final specifications of the constructed collimators varied slightly from the calculated designs due to manufacturing constraints. Table I compares the specifications of the original standard collimators and new optimized collimators, and lists their respective theoretical geometric efficiencies and theoretical spatial resolutions at a distance of 3 cm from the collimator face. The constructed optimized collimators were registered to individual pixels. The choice of collimator material (tungsten versus lead) was dictated by pixel size. For the 1.6 mm pixel on the GMI system, optimal sensitivity was achieved using a tungsten design. Tungsten permitted use of thinner septa and increased sensitivity relative to lead.[12] For the 2.5 mm pixel size of the GE system, the dead space between pixels was larger and a lead design was employed as no advantage in sensitivity was gained through use of tungsten. For both designs, hole length was shortened and septal thickness increased relative to standard collimation.

#### *II.B.2. Energy acceptance window*

The standard energy acceptance window used with Tc-99m sestamibi is 126–154 keV, which is ±10% of the 140 keV photopeak. The semiconductor CZT detects gamma rays by absorbing energy of incident photons, which creates a cloud of

TABLE I. Specifications of standard collimators and optimized low-dose collimators for each CZT detector.

| Detector | CZT pixel size (mm) | Collimator | Hole shape | Material | Hole length (cm) | Hole diameter[a] (mm) | Septal thickness (mm) | Theoretical geometric efficiency[b] | $b_{min}$ (cm)[c] | Theoretical $R_C$ at b = 3 cm[d] |
|---|---|---|---|---|---|---|---|---|---|---|
| GMI LumaGem | 1.6 | GMI Standard | Hexagonal | Lead | 2.50 | 2.54 | 0.30 | $6.1 \times 10^{-4}$ | 1.55 | 5.7 |
| | | GMI Optimized | Square, registered | Tungsten | 0.94 | 1.225 | 0.375 | $9.0 \times 10^{-4}$ | 0.758 | 5.4 |
| GE Discovery NM 750b | 2.5 | GE Standard | Square, registered | Lead | 3.47 | 2.26 | 0.24 | $2.9 \times 10^{-4}$ | 2.10 | 4.3 |
| | | GE Optimized | Square, registered | Lead | 2.10 | 2.10 | 0.40 | $6.0 \times 10^{-4}$ | 1.45 | 4.5 |

[a]For both square and hexagonal holes, the hole diameter is measured from parallel side to parallel side.
[b]Geometric efficiency was calculated using Eq. (14-7) from Ref. 25: $g = K^2(d/l_e)^2[d^2/(d+t)^2]$ where $K \sim 0.26$ for hexagonal arrays and $K \sim 0.28$ for square arrays.
[c]The distance beyond which a source can be seen by adjacent collimator holes is $b_{min}$.
[d]Collimator spatial resolution, $R_C$ was calculated as a function of distance from the collimator, b, using Eq. (14-6) from Ref. 25: $R_C = d(l_e + b)/l_e$.

electron-hole pairs or charges in the CZT. The number of charges collected by the CZT anode allows the detector to discriminate the energy of each incident photon. Although CZT has excellent energy discrimination, the energy spectrum of a CZT detector has a skewed appearance where a proportion of counts are shifted to lower energies, also known as the "tailing effect."

There are three main factors contributing to the tailing effect: (1) charge collection is weaker at pixel boundaries than in the centers; (2) there is a depth-of-interaction dependence in CZT; and (3) some charges are shared across multiple pixels. All of these processes result in incomplete charge collection, and consequently, a proportion of absorbed photons are misregistered at lower-than-actual energies.

Our previous work examining the MBI energy spectrum has found that approximately 60% of counts across the entire spectrum (open energy window) are registered at reduced energies.[17] Some of these photons may have a small enough change in their registered energy such that they are still accepted within the standard energy window. The recovery of other photons would require wider energy windows, and even then all of the photons would not be captured unless an open energy window as used. Regardless of the energy window used, one way to lessen some of the tailing effects is to register the collimator septa with the pixel boundaries, which would minimize the contribution of two of the mentioned tailing causes: weaker charge collection at pixel boundaries and charge sharing between adjacent pixels.

Using equations provided by Iniewski *et al.*, we calculated the contribution of charge sharing between adjacent pixels and found that 14%–15% of all incoming 140 keV photons are registered at lower energies due to charge sharing between adjacent pixels, which could degrade spatial resolution; however, it is unknown what portion of these charged-shared events are captured in a given energy window.[18]

A compromise must be made between widening the energy window to recover tailed primary events while keeping it narrow enough to reject the increased scatter events at lower energies. Our previous Monte Carlo work also showed that the number of scattered events detected in an MBI image is relatively low compared to that observed in conventional nuclear medicine. With MBI, only approximately 14% of events acquired in a standard 126–154 keV energy window are non-photopeak events (have undergone scatter); ~18% of those, or approximately 2.5% of all events in that standard energy window originated in the torso and scattered into the MBI image.[17] This is because when MBI is performed under light compression with a shielded dedicated gamma camera, the breast is uniquely positioned where it is isolated from the rest of the body, except at the chest-wall edge, and is of a relatively small thickness (average of 6 cm) of tissue. We therefore hypothesized that we could widen the energy acceptance window to capture more photopeak events that had undergone tailing while allowing an acceptable increase in scattered events. From prior modeling of patient energy spectra, we selected a lower bound of the widened energy window of 110 keV. We determined this lower energy bound would have the following effects: 1.3 times the number of photopeak counts would be collected, the total proportion of all scattered counts in the image would increase from 14% to about 25%, and the proportion of scattered counts that originated in the torso, including heart and liver, would increase from 2.5% to 10%.[17] Figure 1 displays the components of the simulated MBI energy spectra for CZT with energy resolution of 3.8% at 140 keV. It can be seen that at an energy of ~110 keV, the number of photopeak events begin to exceed the number of scatter counts originating from the torso (i.e., outside the breast).

## II.C. Evaluation of sensitivity improvement methods in phantoms

### II.C.1. Imaging parameters

All measurements of system sensitivity, system spatial resolution and lesion contrast-to-noise ratio (CNR) described below were performed under four imaging configurations on each system. These configurations were (a) standard collimation and standard (126–154 keV) energy window, (b) standard collimation and wide energy window (110–154 keV), (c) optimized collimation and standard energy window, and (d) optimized collimation and wide energy window.

### II.C.2. System sensitivity

System sensitivity was measured using the standard NEMA (National Electrical Manufacturers Association) method.[19] A thin layer of water with a known amount of Tc-99m sestamibi was placed in a plastic Petri dish and imaged for 2 min. The

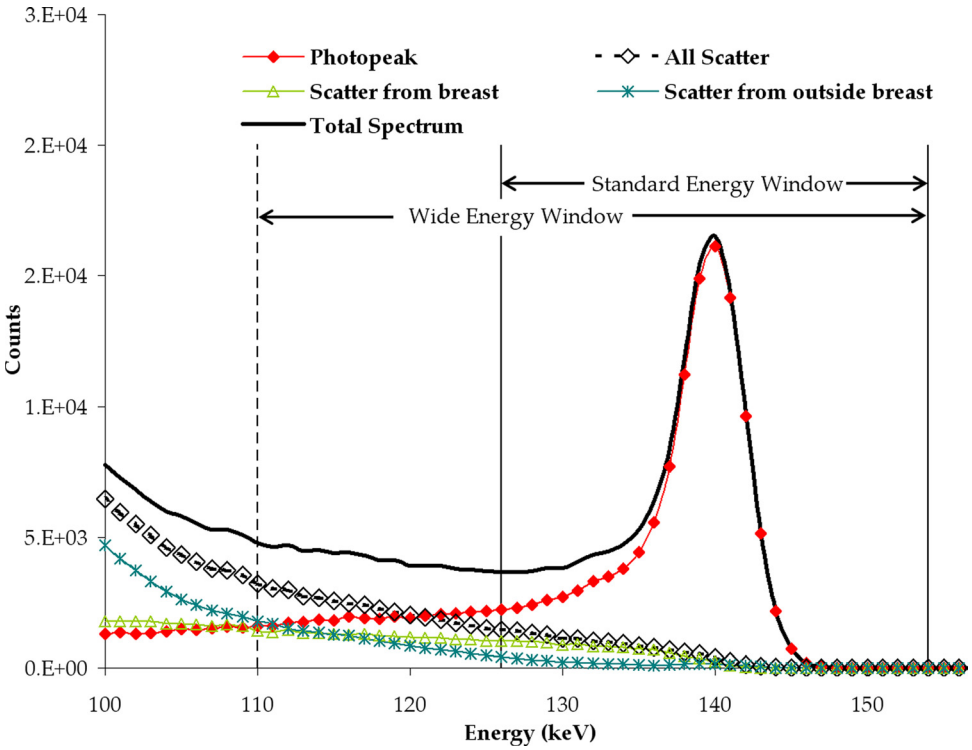


FIG. 1. Components of the simulated energy spectrum for CZT (with 3.8% energy resolution) for an MBI acquisition using standard energy window and wide energy window.

total counts in a region of interest (ROI) surrounding the Petri dish were measured, decay corrections were applied, and sensitivity was expressed in units of counts/min/kBq.

### II.C.3. Spatial resolution

Spatial resolution of each detector was measured using a Tc-99m point source created in the tip of a capillary tube with internal diameter of 0.5 mm. The source was placed at distances of 0.3, 1, 2, 3, 4, and 5 cm from the collimator face and imaged for a minimum of 30 k counts.

Using MATLAB (MathWorks, Natick, MA), a 3D Gaussian surface was fit to the pixel intensities of each point source image. The full-width at half-maximum (FWHM) of each Gaussian surface was calculated using the following equation:

$$\mathrm{FWHM} = 2\sqrt{2\ln(2)} \cdot \sigma, \quad (1)$$

where sigma is the standard deviation of the Gaussian surface. A linear least-squares fit was applied to the FWHM measurements as a function of distance from the collimator. A 95% confidence interval for uncertainty in the linear fit was calculated according to the method used by Altman and Gardner.[20]

### II.C.4. Lesion contrast-to-noise ratio

A phantom, comprising a 20 cm × 20 cm × 20 cm plastic box with a moveable plastic jig on which 16 glass spheres were mounted, was used to simulate tumors in the breast. The 16 spheres comprised four sets of spheres with internal diameters $4.8 \pm 0.2$, $5.9 \pm 0.3$, $8.0 \pm 0.2$, and $9.2 \pm 0.1$ mm and wall thickness of 0.6 mm. The box was filled with water to a depth of 6 cm, and the spheres and box were filled with Tc-99m at a ~20:1 activity concentration ratio. We have previously used phantom simulations of breast tumors with various uptake concentrations and found that a 20:1 ratio provides tumor detectability consistent with that observed in our clinical experience.[21] The spheres were imaged at distances of 1, 3, and 5 cm from the collimator face.

In our experience with the two CZT detectors under study, we have found that clinical MBI studies are considered of acceptable quality when the count density reaches ~800 counts/cm$^2$ or more. This count density corresponds to that previously reported for images acquired using the standard collimation and energy window; median count density was 873 counts/cm$^2$ for standard acquisitions acquired for 10 min following 740 MBq injection.[15]

To assess the impact of reduced counts on lesion detection, breast phantom images were acquired in dynamic mode, such that frames could be summed to create range of count densities. Using the standard collimation and energy window, a ten-frame acquisition of the phantom was performed until the total average count density in a background region reached 800 counts/cm$^2$ (corresponding to the clinically observed count density for 10 min-acquisitions following 740 MBq injection), or 80 counts/cm$^2$ within each of the 10 frames. From the dynamic acquisitions, the appropriate number of frames was summed to create images ranging from 80 to 800 counts/cm$^2$. Breast phantom images were then acquired using the optimal collimation and optimal energy window for the same acquisition duration as the standard acquisition, with a small increase in total acquisition duration to adjust for radioactive decay during the time elapsed between acquisitions.

In each image, tumor CNR, defined as

$$\mathrm{CNR} = \frac{\text{average tumor pixel count} - \text{average background pixel count}}{\text{standard deviation of background pixel counts}}, \quad (2)$$

was measured on each lesion in the breast phantom and results were averaged for each of the four sets of sizes. A CNR value of 1 therefore represents when tumor intensity is equal to the sum of the background intensity and its noise (standard deviation of background). Tumor counts were obtained from circular ROIs with diameter matching that of the internal diameter of each sphere and centered on each lesion. Prior to measuring counts for the CNR measurements, the LumaGem images (pixel size = 1.6 mm) were first resampled using a cubic interpolation such that its pixel size was identical to that of Discovery NM 750b (2.5 mm). The cubic interpolation models the local distribution of pixel values in the neighborhood of the pixel being interpolated using a windowed sinc function. This interpolation was performed in order to allow CNR measurements across systems that were independent of pixel size.

A paired, two-tailed t-test was performed to compare the CNR measurements of each of the four lesion sizes obtained with standard collimator and energy window versus the other settings of collimator and energy window for both detector systems. An alpha level of 0.05 was used to determine if changes in CNR with optimal collimation and/or wide energy window was significant.

#### *II.C.5. Image content in widened energy window*

In order to determine the additional count information provided by widening the energy acceptance window, we examined images of the breast phantom (acquired as detailed above) and subtracted the standard energy window image from the wide energy window image. All images were acquired for the same acquisition time with correction for radioactive decay. This process effectively allowed us to create an image of counts in the 110–125 keV range and assess whether the additional counts contained useful spatial information.

## III. RESULTS

### III.A. System sensitivity

The system sensitivity measurements for each combination of detector, collimator, and energy window are shown in Table II. With optimized collimation, the gain in count sensitivity was 2.9 for the LumaGem and 2.1 for the Discovery NM 750b detectors. An additional gain of 1.3 in counts was achieved with a widened energy window on both detectors. When both optimized collimation and widened energy window were applied, the overall gain in system sensitivity was 3.6 for the LumaGem and 2.8 for the Discovery NM 750b.

### III.B. Spatial resolution

The measured spatial resolution of each detector with its respective collimators, in FWHM of the Tc-99m point source, is shown as a function of source-to-collimator distance in Fig. 2. As measurements of spatial resolution can be influenced by placement of the point source relative to septal junctions of the collimator, a best fit line between the measured points is shown for each collimator. Greater variability in measurements was observed for the standard hexagonal-hole collimator on the LumaGem, as Moiré interference patterns caused by overlapping of the hexagonal collimator septa with square pixels impacted the shape of pixel intensity profiles.

This linear fit was noted to fall below each detector's intrinsic pixel size when the line was extrapolated to the collimator surface (distance = 0). In previous work, we have discussed an important near-field collimator parameter called $b_{min}$, the distance beyond which a source of radioactivity can be detected in adjacent collimator holes.[12] At distances closer to the collimator face than $b_{min}$, the radiation passes through only one collimator hole. We have demonstrated that inside of $b_{min}$ the measured spatial resolution does not have a linear relationship with distance but plateaus

TABLE II. Count sensitivity measurements for standard and low-dose collimation and energy window settings on each CZT detector.

| Detector | Collimator | Energy window | Sensitivity (counts/min/kBq) | Relative gain[a] |
|---|---|---|---|---|
| GMI LumaGem | GMI Standard | Standard, 140 ± 10% | 8.43 | 1.0 |
| | GMI Optimized | Standard 140 ± 10% | 24.46 | 2.9 |
| | GMI Standard | Wide, 110–154 keV | 10.57 | 1.3 |
| | GMI Optimized | Wide, 110–154 keV | 30.59 | 3.6 |
| GE Discovery NM 750b | GE Standard | Standard, (140 ± 10)% | 6.86 | 1.0 |
| | GE Optimized | Standard (140 ± 10)% | 14.43 | 2.1 |
| | GE Standard | Wide, 110–154 keV | 8.95 | 1.3 |
| | GE Optimized | Wide, 110–154 keV | 19.05 | 2.8 |

Note: GMI = Gamma Medica-Ideas; GE = General Electric.
[a]Gain relative to the count sensitivity of each system with their respective standard collimator and standard energy window.

so that FWHM is essentially the collimator hole size. In the systems evaluated here with registered collimators, the hole size is slightly less than the detector pixel size, so the measured resolution within $b_{min}$ approximates the pixel size.

For each detector, comparison of the 95% confidence intervals of the linear fits did not demonstrate a statistical difference in spatial resolution between optimal and standard collimators. According to the best fit line, at a distance of 3 cm from the collimator face, the LumaGem's spatial resolution was estimated as 4.8 mm with the standard collimator and 5.6 mm with the optimized collimator. Spatial resolution at 3 cm of the Discovery NM 750b was 4.4 mm with the standard collimator and 4.6 mm with the optimized collimator. No change in the measured FWHM of the point source was observed with use of the widened energy window rather than the standard energy window.

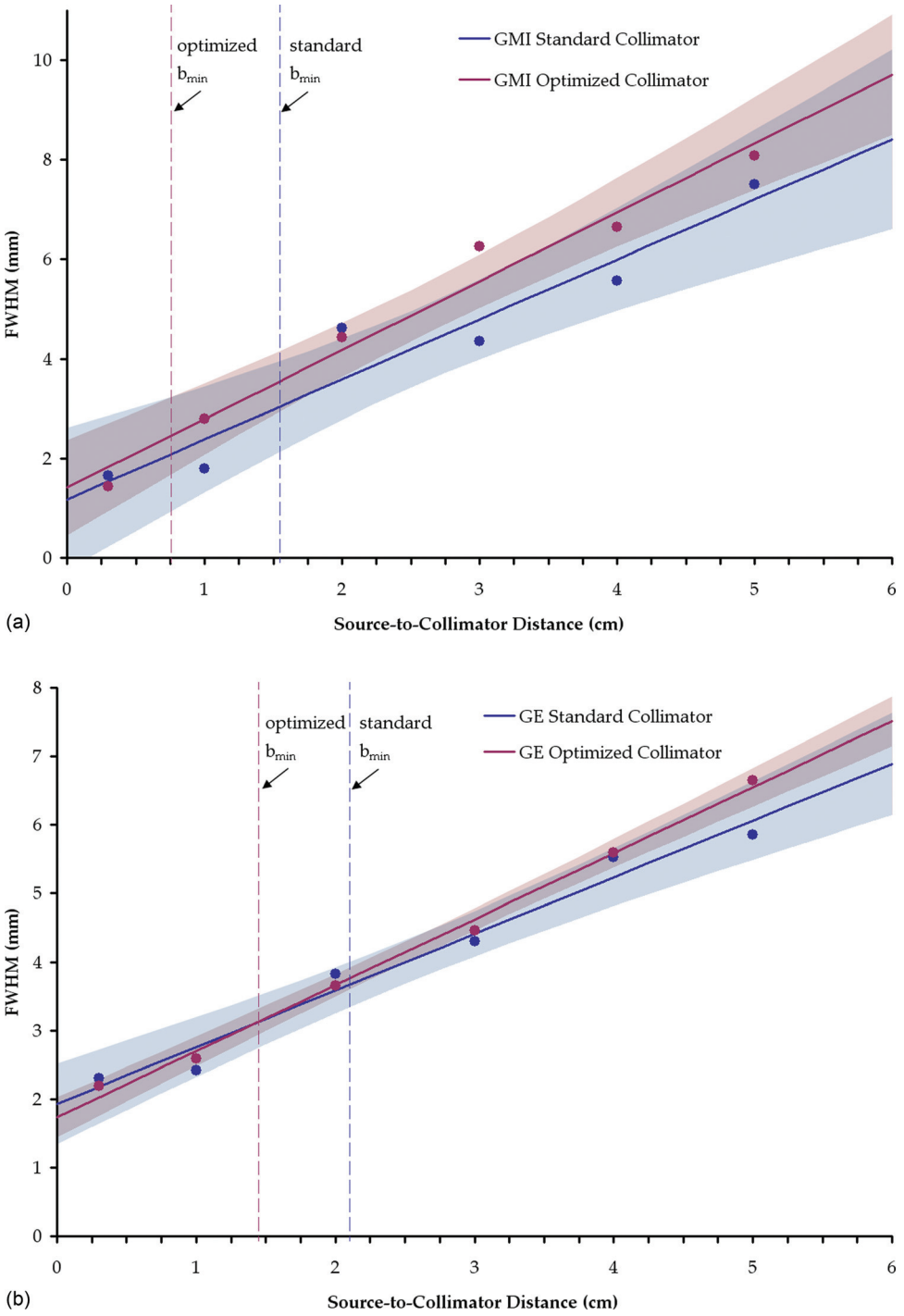


FIG. 2. System spatial resolution of the LumaGem detector [shown in (a)] and the Discovery NM 750b detector [shown in (b)] with their respective standard and optimal collimators. A 95% confidence interval of uncertainty of the linear fit is indicated. Vertical lines indicated $b_{min}$, the distance below which spatial resolution plateaus to equal collimator hole size.

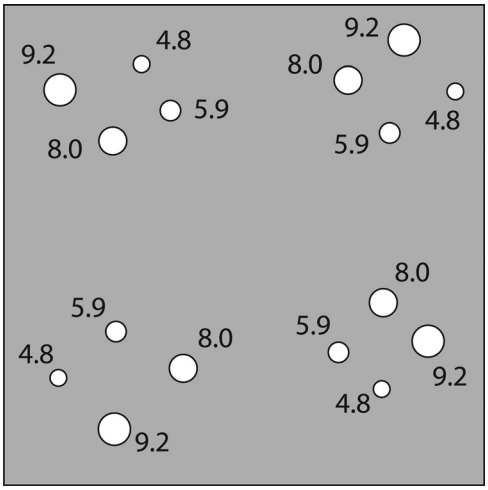


FIG. 3. Schematic of tumor placement within the breast phantom. Tumor diameter given in millimeter.

### III.C. Lesion contrast-to-noise ratio

A schematic of tumor placement within the breast phantom is shown in Fig. 3. Figure 4 compares the effects of standard and new collimation/energy window settings on the appearance of breast phantom images acquired on both systems. In Fig. 5, CNR is shown as a function of lesion size for the count densities corresponding to a 148 MBq dose level.

For acquisitions performed on the LumaGem system the calculated 148 MBq dose level corresponded to a count density of 160 counts/cm$^2$ when the standard GMI collimator and energy window settings were used. At this count density and a lesion depth of 1 cm [Fig. 5(a)], the standard collimator and energy window settings resulted in lesion CNR high enough to permit lesion detection (CNR $>$ 1) for the largest two lesions (8.0 and 9.2 mm) and borderline detectability of the 5.9 mm lesion. At lesion depth of 3 cm [Fig. 5(b)], the standard collimator and energy window allowed detection of the 9.2 mm lesion and borderline detectability of the 8.0 mm lesion. Use of any combination of the optimized collimator and/or wide energy window resulted in significantly improved CNR compared to standard collimator/standard energy window for the largest two lesions. A trend in CNR improvement with collimator and energy window changes was observed for the 5.9 mm lesion, but was not significant for measurements at the 1 cm depth, and did not result in meeting the detectability threshold of CNR = 1 at the 3 cm depth.

For acquisitions performed on the Discovery NM 750b, the calculated 148 MBq dose level also corresponded to a count density of 160 counts/cm$^2$ when the standard GE collimator and energy window were used. At this dose level, the 8.0 and 9.2 mm lesions were detectable (CNR $>$ 1) and the 5.9 mm lesion had borderline detectability for both depths of 1 and 3 cm. Use of any combination of the optimized collimator and/or wide energy window provided significantly improved CNR for the 5.9–9.2 mm lesions at a depth of 1 cm [Fig. 5(c)]. At a depth of 3 cm, the only significant improvement in CNR was observed for the 8.0 and 9.2 mm lesions with use of both the optimized collimator and wide energy window [Fig. 5(d)].

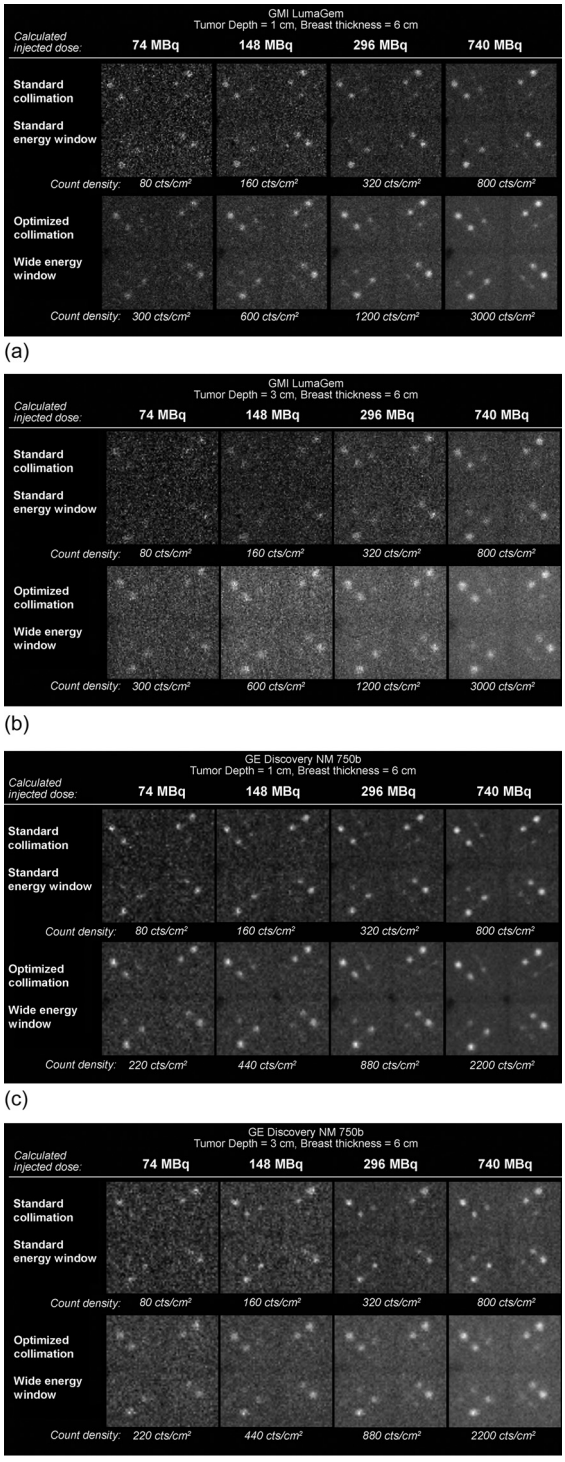


FIG. 4. Images of breast phantom acquired on the LumaGem and Discovery NM 750b CZT detectors using their respective standard collimators and a standard 126–154 keV energy window (top row) and respective optimized collimators and wide (110–154 keV energy window (bottom row). Activity concentration ratio in tumors versus background was ~20:1. Images from the LumaGem are shown in (a) with tumors were placed at a depth of 1 cm and in (b) depth was 3 cm from the collimator face. Images from Discovery NM 750b are shown in (c) with tumors at 1 cm depth and in (d) with tumors at 3 cm depth. The highest simulated count density with standard settings of 800 counts/cm$^2$ was chosen to match that observed in patient studies performed with injection of 740 MBq Tc-99m sestamibi. A proportionally decreased dose was calculated to correspond with phantom images of decreased count densities.

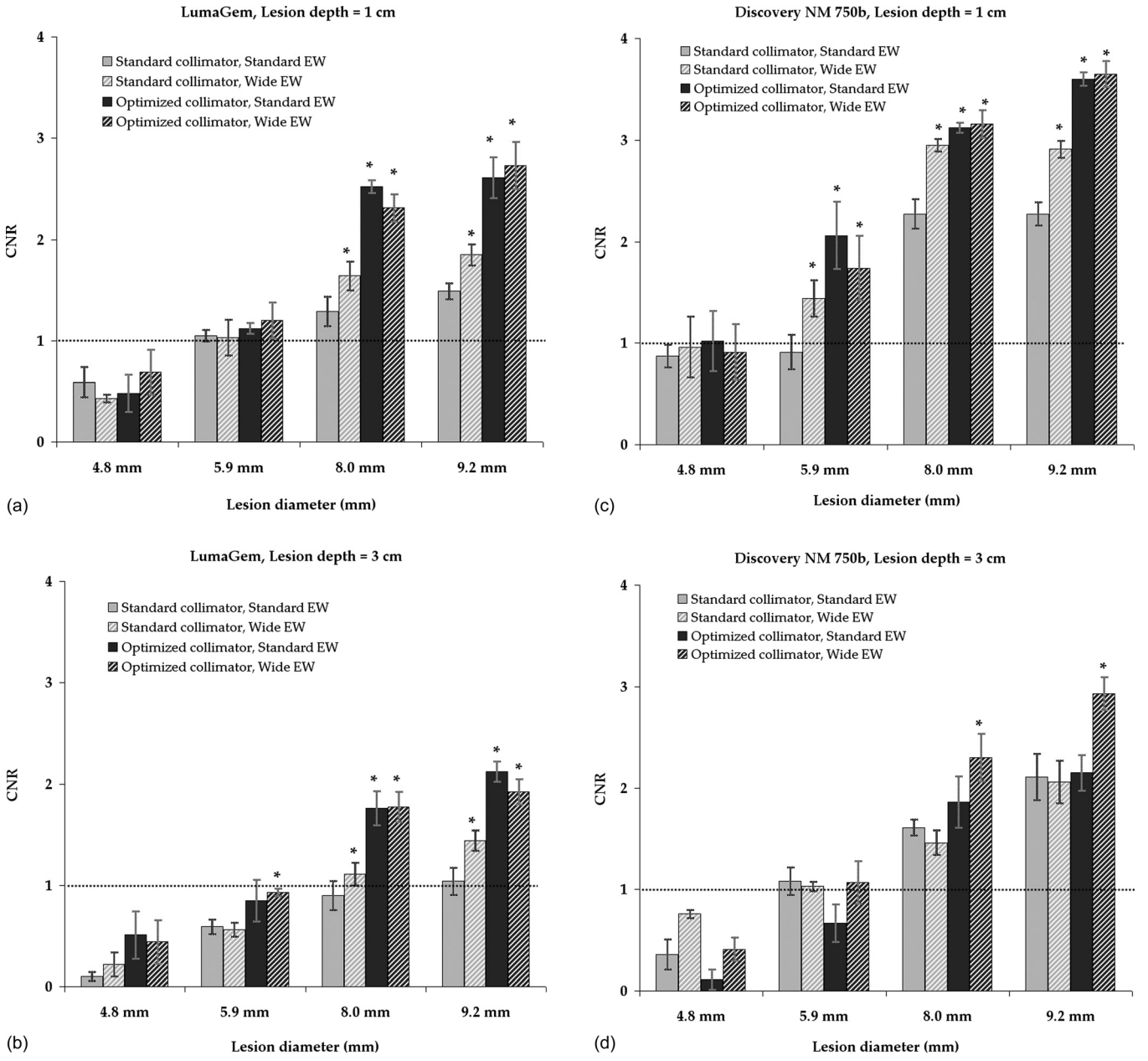


FIG. 5. Lesion CNR as a function of lesion size measured on breast phantom images with respective count densities representing a 148 MBq dose of Tc-99m sestamibi. Images were acquired on LumaGem at lesion depths of 1 and 3 cm from the collimator face [shown in (a) and (b)] and Discovery NM 750b also at lesion depths of 1 and 3 cm [shown in (c) and (d)] with each combination of standard and optimized collimators and standard and wide energy windows. Total simulated breast thickness was 6 cm. Error bars represent the standard error of the CNR measurements. Lesions were considered detectable at a CNR greater than 1, as indicated by the dotted line. Significantly improved CNR relative to that obtained with standard collimator and standard energy window is noted with "*."

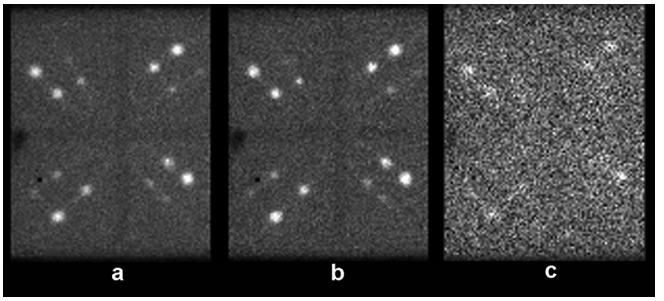


FIG. 6. Breast phantom images acquired on the LumaGem system performed using (a) wide energy window (110–154 keV), (b) standard energy window (126–154 keV), and (c) their difference.

On both detector systems and both depths studied, the CNR of the 4.8 mm lesion was below the threshold of detectability (CNR $< 1$) for images acquired with count densities at or lower than those representing a 148 MBq dose. At a 5 cm depth, no statistical difference in CNR for any lesion size was observed between acquisitions with standard settings or optimized collimators and/or wide energy window.

### III.D. Image content in widened energy window

Figure 6 shows examples of breast phantom images acquired using a wide energy window, a standard energy window, and their difference. The difference image demonstrates

that photopeak events are present in the 110–125 keV range. The true effect of the widened energy window on scatter contribution in a patient may be underestimated in these phantom experiments as it does not account for the variable effect of scatter from activity in the heart and liver.

## IV. DISCUSSION AND CONCLUSION

With implementation of new registered collimators optimized for count sensitivity and use of an asymmetrical wide energy acceptance window, overall system sensitivity was increased by a factor of 2.8–3.6 in NEMA sensitivity measurements. These gains in count sensitivity could potentially permit an inversely proportional reduction in the administered dose of Tc-99m sestamibi required for acceptable image quality in clinical MBI studies. The gains in sensitivity are achieved with a small loss in spatial resolution, particularly at source-to-collimator distances greater than 3 cm. However, the use of opposing dual-head detectors ensures that the greatest distance a lesion may be from either collimator is half the lightly compressed breast thickness, which is on average 3 cm as observed in clinical studies. The spatial resolution of the systems in the 0–3 cm near-field ranged from 1.6 mm (pixel size) to 5.6 mm for the LumaGem and from 2.5 cm (pixel size) to 4.4 mm for the Discovery NM 750b. Degradation of resolution beyond distances of 3 cm should have minimal impact on the ability of the system to detect lesions ~5 mm or greater in size.

As seen in Figs. 4 and 5, the changes to collimation and energy window allowed adequate CNR and spatial resolution to permit reliable detection of 8 and 9.2 mm tumors at depths of 1 and 3 cm, and the detection of 5.9 mm tumors at the closer depth of 1 cm, at a count density calculated to correspond to injected dose of 148 MBq Tc-99m sestamibi. The detection of breast tumors when they are less than 1 cm in size is a goal for a screening technique as this threshold is an important prognostic factor for disease-free survival.[22] However, our findings indicate that detection of lesions far from the collimator (~5 cm) and lesions smaller than 5 mm in size will be challenging at reduced count densities.

Due to manufacturing constraints, there were slight differences in hole length and septal thickness between the optimal collimator previously designed in Weinmann *et al.*[12] and the actual constructed collimators which were implemented in this work. After accounting for these differences, we still observed some differences between the measured values of system sensitivity and spatial resolution with those derived from theoretical calculations (Table I). These differences may be attributed to the fact that standard collimator equations do not account for the effect of coupling a pixilated detector with a registered collimator nor for sources in the near-field range of 0–2 cm from the collimator. A second factor which influences count sensitivity and resolution is the small gap (~2 mm) present between the actual collimator and detector, a factor which is not typically considered to have an impact. However, the optimized collimation for LumaGem has an extremely short bore length of 9.4 mm, likely making the relative contribution of this gap more important for this system. Therefore, it appears that registration of collimator holes with individual pixels and the small gap between collimator and detector yields greater gains in sensitivity and slightly poorer spatial resolution than can be appreciated by standard theoretical calculations.

From a practical perspective, the new collimators (particularly those constructed with tungsten) are likely to be more expensive than conventional hexagonal-hole collimators. However, we believe that the benefits of increased sensitivity and the potential to reduce administered dose outweigh the small overall increase in the cost of the imaging system.

The potential benefits of the wider energy window on count sensitivity are peculiar to CZT due to the tailing phenomenon. Future improvements to the application-specific integrated circuits (ASICs) of the CZT modules will reduce the tailing effect deficiencies of CZT, thereby providing improved count sensitivity without the need for a wider energy window. The use of a wider energy window does allow additional scattered counts in the image, and a limitation in this phantom work was the lack of a source to simulate scatter from the adjacent torso, including radiotracer uptake in the heart and liver that may reduce lesion contrast close to the chest-wall edge of the breast. However, from Monte Carlo simulations, we observed that most of the scattered photons in the 110–154 keV energy window originated in the breast itself and did not come from the torso. This issue is further explored in Part II of this work conducted in patients.

In addition to the count sensitivity improvement methods implemented here, additional postacquisition processing techniques may lead to further improvements in image quality of low-dose gamma imaging techniques such as MBI.[13,14,23] Judy *et al.* have shown that some image combination methods for conjugate breast views may improve lesion detectability by improving lesion contrast and signal-to-noise ratio.[23] Image enhancement techniques using denoising algorithms and new methods for combining data from individual detector heads that retain image contrast have also been shown to improve image quality in low-count data.[13,14] Algorithms such as the Wide Beam Reconstruction technique that are routinely used in clinical nuclear medicine to enhance image quality through noise reduction and resolution recovery[24] are also currently under evaluation for MBI in our laboratory. While the impact of the above techniques has yet to be ascertained, their implementation could potentially yield an improvement in resolution for a given sensitivity.

We conclude that implementation of new collimation optimized for count sensitivity and widened energy window have improved MBI image quality by substantially increasing count sensitivity and making a measurable increase in tumor CNR for lesions over 0.8 cm. These count sensitivity improvements may allow MBI to be performed with doses of 148 MBq Tc-99m sestamibi.

## ACKNOWLEDGMENTS

This research was supported by Mayo Clinic Foundation; National Institutes of Health (R21R33 CA 128407). The

Mayo Foundation and authors of this work (C. B. Hruska, A. L. Weinmann, and M. K. O'Connor) obtain royalties from licensing arrangements between the Mayo Foundation and Gamma Medica-Ideas.

[a]Author to whom correspondence should be addressed. Electronic mail: hruska.carrie@mayo.edu; Telephone: 507-284-9599; Fax: 507-266-4461.

[1]C. B. Hruska, J. C. Boughey, S. W. Phillips, D. J. Rhodes, D. L. Wahner-Roedler, D. H. Whaley, A. C. Degnim, and M. K. O'Connor, "Scientific impact recognition award: Molecular breast imaging: A review of the Mayo Clinic experience," **196**, 470–476 (2008).

[2]M. O'Connor, D. Rhodes, and C. Hruska, "Molecular breast imaging," Expert Rev. Anticancer Ther. **9**, 1073–1080 (2009).

[3]M. T. Mandelson, N. Oestreicher, P. L. Porter, D. White, C. A. Finder, S. H. Taplin, and E. White, "Breast density as a predictor of mammographic detection: Comparison of interval- and screen-detected cancers," J. Natl. Cancer Inst. **92**, 1081–1087 (2000).

[4]T. M. Kolb, J. Lichy, and J. H. Newhouse, "Comparison of the performance of screening mammography, physical examination, and breast ultrasound and evaluation of factors that influence them: An analysis of 27,825 patient evaluations," Radiology **225**, 165–175 (2002).

[5]P. A. Carney, D. L. Miglioretti, B. C. Yankaskas, K. Kerlikowske, R. Rosenberg, C. M. Rutter, B. M. Geller, L. A. Abraham, S. H. Taplin, M. Dignan, G. Cutter, and R. Ballard-Barbash, "Individual and combined effects of age, breast density, and hormone replacement therapy use on the accuracy of screening mammography," Ann. Intern Med. **138**, 168–175 (2003).

[6]D. S. M. Buist, P. L. Porter, C. Lehman, S. H. Taplin, and E. White, "Factors contributing to mammography failure in women aged 40–49 years," J. Natl. Cancer Inst. **96**, 1432–1440 (2004).

[7]E. D. Pisano, R. E. Hendrick, M. J. Yaffe, J. K. Baum, S. Acharyya, J. B. Cormack, L. A. Hanna, E. F. Conant, L. L. Fajardo, L. W. Bassett, C. J. D'Orsi, R. A. Jong, M. Rebner, A. N. A. Tosteson, and C. A. Gatsonis for the DMIST Investigators Group, "Diagnostic accuracy of digital versus film mammography: Exploratory analysis of selected population subgroups in DMIST," Radiology **246**, 376–383 (2008).

[8]R. E. Hendrick, "Radiation doses and cancer risks from breast imaging studies," Radiology **257**, 246–253 (2010).

[9]National Research Council, *BEIR VII: Health Risks from Exposure to Low Levels of Ionizing Radiation* (National Academies, Washington, DC, 2006).

[10]M. K. O'Connor, H. Li, D. J. Rhodes, C. B. Hruska, C. B. Clancy, and R. J. Vetter, "Comparison of radiation exposure and associated radiation-induced cancer risks from mammography and molecular imaging of the breast," Med. Phys. **37**, 6187–6198 (2010).

[11]M. J. Yaffe and J. G. Mainprize, "Risk of radiation-induced breast cancer from mammographic screening," Radiology **258**, 98–105 (2011).

[12]A. L. Weinmann, C. B. Hruska, and M. K. O'Connor, "Design of optimal collimation for dedicated molecular breast imaging systems," Med. Phys. **36**, 845–856 (2009).

[13]C. Hruska, A. Weinmann, N. Khaylova, A. Manduca, and M. O'Connor, "Dose reduction methods for molecular breast imaging," J. Nucl. Med. **50**, 1526 (2009).

[14]M. K. O'Connor, C. B. Hruska, A. Weinmann, A. Manduca, and D. J. Rhodes, "Development of radiation dose reduction techniques for cadmium zinc telluride detectors in molecular breast imaging," Proc. SPIE **7806**, 780603 (2010).

[15]C. B. Hruska, S. W. Phillips, D. H. Whaley, D. J. Rhodes, and M. K. O'Connor, "Molecular breast imaging: Use of a dual-head dedicated gamma camera to detect small breast tumors," AJR, Am. J. Roentgenol. **191**, 1805–1815 (2008).

[16]M. K. O'Connor, S. W. Phillips, C. B. Hruska, D. J. Rhodes, and D. A. Collins, "Molecular breast imaging: Advantages and limitations of a scintimammographic technique in patients with small breast tumors," Breast J. **13**, 3–11 (2007).

[17]C. B. Hruska and M. K. O'Connor, "A Monte Carlo model for energy spectra analysis in dedicated nuclear breast imaging," IEEE Trans. Nucl. Sci. **55**, 491–500 (2008).

[18]K. Iniewski, H. Chen, G. Bindley, I. Kuvvetli, and C. Budtz-Jorgensen, "Modeling charge-sharing effects in pixellated CZT detectors," IEEE Nucl. Sci. Symp. Conf. Rec. **6**, 1082–3654 (2007).

[19]National Electrical Manufacturers Association, *NEMA Standards Publication NU 1-2007: Performance Measurements of Gamma Cameras* (National Electrical Manufacturers Association, Rosslyn, VA, 2007).

[20]D. G. Altman and M. J. Gardner, "Calculating confidence intervals for regression and correlation," BMJ **296**, 1238–1242 (1988).

[21]C. B. Hruska and M. K. O'Connor, "Effect of collimator selection on tumor detection for dedicated nuclear breast imaging systems," IEEE Trans. Nucl. Sci. **53**, 2680–2689 (2006).

[22]A. L. Abner, L. Collins, G. Peiro, A. Recht, S. Come, L. N. Shulman, B. Silver, A. Nixon, J. R. Harris, S. J. Schnitt, and J. L. Connolly, "Correlation of tumor size and axillary lymph node involvement with prognosis in patients with T1 breast carcinoma," Cancer **83**, 2502–2508 (1998).

[23]P. G. Judy, Z. Gong, N. L. Dinion, B. L. Welch, T. St Saviour, D. Kieper, S. Majewski, B. Kross, J. Proffitt, A. V. Stolin, M. J. More, M. B. Williams, "Analysis of image combination methods for conjugate breast scintigraphy" IEEE Trans. Nucl. Sci. **57**, 1146–1154 (2010).

[24]R. Druz, L. Phillips, M. Chugkowski, L. Boutis, B. Rutkin, and S. Katz, "Wide-beam reconstruction half-time SPECT improves diagnostic certainty and preserves normalcy and accuracy: A quantitative perfusion analysis" J. Nucl. Cardiol. **18**, 52–61 (2011).

[25]S. R. Cherry, J. A. Sorenson, and M. E. Phelps, *Physics in Nuclear Medicine*, 3rd ed. (Saunders, Philadelphia, 2003).